Tuning the Electronic Structure of Anatase Through Fluorination

Dario Corradini,* Damien Dambournet, and Mathieu Salanne†

Sorbonne Universités, UPMC Univ Paris 06, CNRS, UMR 8234, PHENIX, Paris, France

A highly fluorinated anatase lattice has been recently reported, providing a new class of materials whose general chemical formula is $Ti_{1-x}\square_x X_{4x} O_{2-4x}$ ($X^- = F^-$ or OH^-). To characterise the complex structural features of the material and the different F environments, we here apply a computational screening procedure. After deriving a polarisable force–field from DFT simulations, we screen in a step-wise fashion a large number of possible configurations differing in the positioning of the titanium vacancies ($\square$) and of the fluorine atoms. At each step only 10 % of the configurations are retained. At the end of the screening procedure, a configuration is selected and simulated using DFT-based molecular dynamics. This allows us to analyse the atomic structure of the material, which is strongly disordered, leading to a strong decrease (by 0.8 eV) of the band gap compared to conventional anatase.

Titanium dioxide, TiO_2, is a widely studied material. TiO_2 has in fact several promising applications, for example in the fields of photocatalysis, green chemistry and energy storage [1–8]. Naturally occurring polymorphs of TiO_2 include rutile, anatase and brookite. Recently, interest in the polymorphs of TiO_2 has been sparked in particular by their possible application as anodic materials in Li ion batteries [9–14]. Fluorinated TiO_2 has also been investigated [15–20] since the presence of F in the compound might improve the sought characteristics of the material [17] or stabilise the highly reactive {001} facets of the anatase crystal [19, 21]. The nature of the fluorinated compound depends strongly on the fluorination technique employed [18, 22]. So far, the stabilisation of fluorine within the anatase lattice of TiO_2 has been poorly understood, probably because of the structural complexity of the fluorinated material.

Pure anatase is a tetragonal crystal, with $c \simeq 2.5a$, and its lattice is characterised by TiO_6 octahedral units. Recently, a novel synthesis technique conducted in our laboratory [23] has led to the preparation of a highly fluorinated anatase material in which fluoride or hydroxide anions replace the oxides in their lattice sites and the resulting charge deficiency is compensated by the formation of a cationic vacancy ($\square$) every four substitutions. The material obtained has thus the general formula $Ti_{1-x}\square_x X_{4x} O_{2-4x}$, where $X^- = F^-$ or OH^- (the amount of F^- may vary depending on the synthesis conditions). Elemental analysis and synchrotron diffraction have revealed the existence of more than 20% cation vacancies. In fact the stoichiometric formula $Ti_{0.78}\square_{0.22}X_{0.88}O_{1.12}$ has been assigned to the most fluorinated composition of the material. By using ^{19}F NMR spectroscopy, it has also been possible to discern three different coordination

modes for the F atoms: $F-Ti_1\square_2$, $F-Ti_2\square_1$ and $F-Ti_3$, highlighting the complex structural arrangement present in the material.

Here we report the results of a computational study of the fully-fluorinated, hydroxide-free material (i.e. $Ti_{0.78}\square_{0.22}F_{0.88}O_{1.12}$) performed in order to better characterise its structural features and the effect of fluorination on the electronic structure. The enormous number of possible structural arrangements of the vacancies and of the F atoms in the anatase structure render the problem untreatable directly by *ab initio* simulations. Therefore we apply a screening procedure on the possible configurations of the material, in the spirit of the emerging high–throughput techniques [24–26], by using classical Molecular Dynamics (MD). Several force–fields have been previously proposed for pure TiO_2 [27–33]. In this work, we use a *polarisable* force–field valid for the pure phase [34] as well as for the fluorinated material. We have extracted its parameters from Density Functional Theory (DFT) simulations, *via* a well-established force and dipole fitting procedure [35, 36]. We have chosen to derive a new force–field instead of using an already available one for TiO_2. This is motivated by the fact that we want the force–field to be compatible with O to F substitutions, as well as with other oxide species, e.g. SiO_2, for future studies [34]. The details on the force–field employed are discussed in Supplementary Section S1, while an additional validation of the parameters involving fluorine atoms is presented in Supplementary Section S2.

In order to generate fluorinated samples starting from the pure TiO_2 anatase, we apply a screening procedure, similar in spirit to what done by Wilmer *et al.* for metal-organic frameworks [37] or by Coudert for zeolites [38]. At the fixed target composition $Ti_{0.78}\square_{0.22}F_{0.88}O_{1.12}$, we consider samples containing F in all possible environments $F - Ti_1\square_2$, $F - Ti_2\square_1$, and $F - Ti_3$, as suggested by NMR [23]. We leave the ratio of F in the different environments free to vary at random. The starting fluorinated structures are generated from the $4 \times 4 \times 2$ pure anatase TiO_2 structure [39] ($Ti_{128}O_{256}$) leading to a system thus composed: $Ti_{100}\square_{28}F_{112}O_{144}$. We generate these configurations by erasing 28 Ti ions at random with no constraints on the creation of adjacent vacancies and

---

* Correspondence and request for materials should be addressed to D. C. (dario.corradini@ens.fr); Current address: Laboratoire PASTEUR, UMR 8640 ENS–CNRS–UPMC Paris 6, Département de Chimie, École Normale Supérieure, 75005 Paris, France.

† Correspondence and request for materials should be addressed to M. S. (mathieu.salanne@upmc.fr).

we randomly substitute 112 O with 112 F. We impose that all F and O must be attached to at least one Ti.

The screening procedure is then initiated. The protocol is as follows:

1) we perform single-point energy calculations on $\simeq 1.5 \cdot 10^5$ configurations; we then retain the $\simeq 1.5 \cdot 10^4$ configurations with the lowest energy for the following step.

2) we perform 0 K geometry optimisations of the atomic positions, keeping the length of the cell vectors fixed; we retain at maximum the $1.5 \cdot 10^3$ configurations with the lowest energy for the following step.

3) we perform 0 K cell optimisations of both the atomic positions and the lengths of the cell vectors, while keeping the box angles fixed at $\alpha = \beta = \gamma = \pi/2$; we retain at maximum the $1.5 \cdot 10^2$ configurations with the lowest energy for the following step.

4) we temper the configurations performing 10 ps NVT runs at finite temperatures from $T_1 = 25$ K to $T_{12} = 300$ K, every $\Delta T = 25$ K. The 15 configurations with the lowest energy at $T_{12} = 300$ K are retained for the following step.

5) for the remaining samples, we perform a series of longer MD simulations at 300 K, first in the NVT and then in the NPT ensemble.

6) we then simulate the configuration with the lowest potential energy for 10 ps using using DFT–based molecular dynamics. We extract structural (bond length, fluorine environments) and electronic (density of states) characteristics of the material from this simulation.

Testing all the starting configurations in a generic, entirely *ab initio* based high-throughput procedure would be impossible. Generally, such studies involve static calculations only since performing *ab initio* MD simulations is computationally too expensive. Nevertheless, it is interesting to test whether our selected configurations, i.e., the 10 configurations remaining at the end of step 5) of the screening procedure would have also been selected if *ab initio* static calculations had been performed. To test this, we take their initial structures and perform a full DFT relaxation. Then we take the same number of random configurations from the starting pool of configurations. We find that the configurations given by the classical screening all have a lower final DFT energy than the ones taken at random. The results of this validation are shown in Supplementary Fig. S7.

Next, we analyse how the initial structural arrangements correlate with the energy of the configurations. The results are shown in Fig. 1. We see that the lowest energies (at 0 K) correlate with a higher fraction
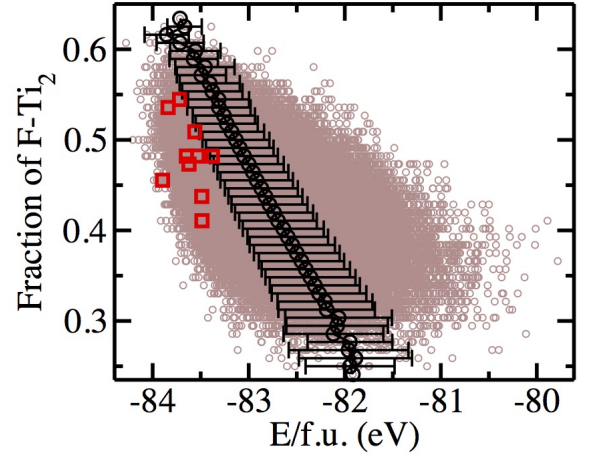
Figure 1. **Energy–structure relation.** Fraction of $F - Ti_2\square_1$ vs. energy of the configuration for the initial configurations at 0 K. The points are represented as small brown circles. For each different value of the fraction of $F-Ti_2\square_1$ we calculate the mean (black circles) and the standard deviation (black bars) of the corresponding energies. We also report the values assumed at this stage by the configurations run at the final screening step (red squares).

of $F - Ti_2\square_1$. This is consistent with previous static DFT calculations performed on a system with only one vacancy and four O/F substitutions [23], which showed that having the F closest to the vacancy stabilises the structure. In Fig. 1 we also report the initial energies of the best configurations given at the end by the screening procedure. We observe that these final screening configurations are found closer to the average F speciation values rather than at the highest $F-Ti_2\square_1$ relative compositions. Some of them have strongly been stabilised during the procedure, showing the importance of taking into account relaxation and thermal effects (see also Supplementary Fig. S8).

In order to compare the structural properties of the material as found in the experiments with our simulations, we plot together the experimental x-ray structure factor $S(k)$ and the one that we calculate from our trajectories using the Ashcroft–Langreth partial structure factors according to the formula:

$$S_{\text{tot}}(k) = \frac{\sum_{\alpha\beta} \sqrt{x_\alpha x_\beta}\, f_\alpha(k) f_\beta(k) S_{\alpha\beta}(k)}{\sum_\alpha x_\alpha f_\alpha^2(k)} \qquad (1)$$

where $\alpha, \beta = Ti, O, F$. x_α are the relative atomic concentrations of atoms of type α, $S_{\alpha\beta}(k)$ are the partial structure factors calculated from the simulation trajectories using

$$S_{\alpha\beta}(k) = \langle \hat{\rho}_\alpha(\mathbf{k}) \hat{\rho}_\beta^*(\mathbf{k}) \rangle \qquad (2)$$

where the dynamic variable $\hat{\rho}_\alpha(\mathbf{k})$ represents the Fourier

component of the atomic density of type α atoms at wave vector $\mathbf{k}$:

$$\hat{\rho}_\alpha(\mathbf{k}) = N_\alpha^{-1/2} \sum_{i=1}^{N_\alpha} \exp\left(\imath \mathbf{k} \cdot \mathbf{r}_i\right) \qquad (3)$$

with $\mathbf{r}_i$ the position of atom i, and N_α the number of atoms of type α in the system. The angular brackets denote a thermal average, which was in practice evaluated as the time average over the whole simulation. Finally, $f_\alpha(k)$ are the k-dependent atomic x–ray scattering factors. They are calculated using the analytic approximation:

$$f_\alpha(k) = c_\alpha + \sum_{i=1}^{4} a_{\alpha,i} \exp\left[-b_{\alpha,i}\left(\frac{k}{4\pi}\right)^2\right] \qquad (4)$$

where the coefficients $a_{\alpha,i}$, $b_{\alpha,i}$ and c_α are taken from Ref. [40] for O^{2-} and from Ref. [41] for Ti^{4+} and F^-. The structure factor calculated from the DFT-based molecular dynamics simulation performed on the final configuration is compared to the experimental signal in Fig. 2. The agreement between the two sets of data is good, taking into account that the experiments have been performed on nanoparticles, which leads to a strong broadening of the peaks, and that part of the fluoride ions are replaced by hydroxide groups. This may also affect the comparison, notwithstanding that F and OH are isoelectronic and thus their contribution to x-ray diffraction should not differ much if they occupy similar sites.
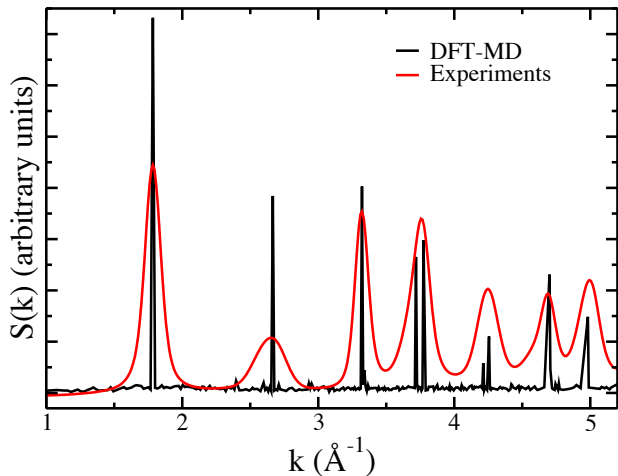
Figure 2. **Structure Factor**. Comparison of the structure factor $S(k)$ at ambient conditions measured in experiments (red line) and calculated from a DFT-based molecular dynamics simulation performed on the configuration selected by the screening procedure (black line).

We also calculate the speciation of fluoride during the DFT-based molecular dynamics simulation. Contrarily to the initial configurations analysed in Fig. 1, the local
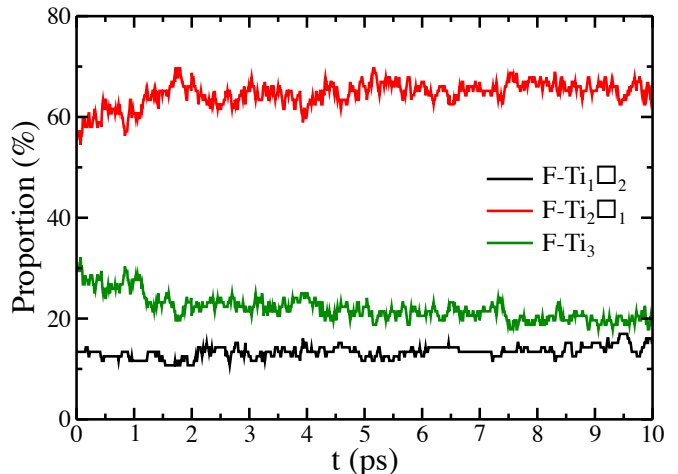
Figure 3. **Fluorine coordination number**. Evolution of the proportion of each coordination mode for the fluorine during the DFT–based MD simulation. The cutoff distance for defining Ti–F neighbour atoms is set to 2.7 Å.

relaxation of the F atoms (especially around the vacancies) leads to a wide distribution of Ti–F distances. It is therefore necessary to introduce a cutoff distance for assigning an environment to the F atoms. In Fig. 3 we show the time evolutions of the concentrations of $F - Ti_1\square_2$, $F - Ti_2\square_1$ and $F - Ti_3$ for a cutoff of 2.7 Å which corresponds to the first minimum of the Ti–F radial distribution function. We observe that after 2 ps of simulation, the concentrations equilibrate around average values of 13/66/21% for $F - Ti_1\square_2$, $F - Ti_2\square_1$ and $F - Ti_3$ respectively. This compares very well with the percentages measured by NMR in the experimental sample, i.e., 13/70/17% [23]. We can therefore conclude that the structure yielded by our screening procedure is realistic. This allows us to analyse it further in order to predict the material properties. We note that the $F - Ti_2\square_1$ average concentration is larger than the corresponding fraction in the initial pool of configurations as shown in Fig. 1, because the fluorine atoms positions relax around the titanium vacancies during the first 2 ps of the simulation. However, no strong lattice rearrangements are observed, as can be seen from Supplementary Fig. S9.

The electronic structure is of particular interest for many applications, since TiO_2-based materials are widely used in photocatalysis. We have therefore calculated the electronic density of states of fluorinated anatase on a series of snapshots extracted from our DFT-based molecular dynamics simulation, and compared it with the case of pure TiO_2 anatase. We have used the hybrid functional HSE06 [42, 43] for these calculations. In agreement with previous works [44], we see in Fig. 4 that the valence band edge of pure TiO_2 anatase is dominated by O $2p$, and the conduction band edge is formed by Ti $3d$. The band gap is much narrower in $F - Ti_1\square_2$, $F - Ti_2\square_1$, by 0.8 eV. Unlike the case of conventional doping with heteroatoms [45], the additional $2p$ states associated with
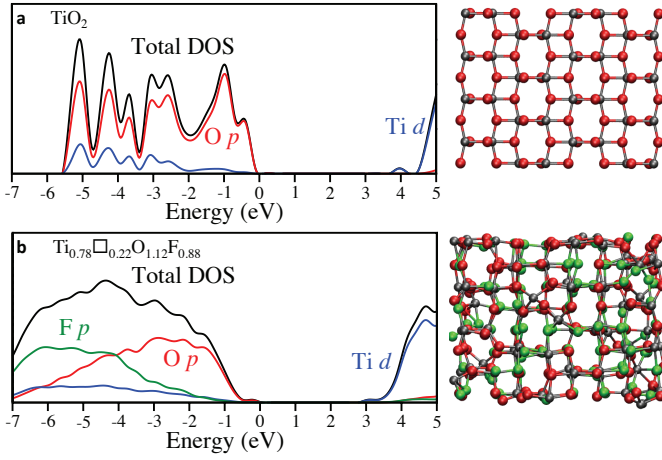
Figure 4. Electronic density of states. Comparison of the total and ion-decomposed density of states of TiO_2(a) and $Ti_{0.78}\square_{0.22}O_{1.12}F_{0.88}$ (b) calculated using the HSE06 functional. Only the main contributions from the decomposition are shown. The plot for $Ti_{0.78}\square_{0.22}O_{1.12}F_{0.88}$ corresponds to the final snapshot of the simulation, shown on the right side. No significant changes have been observed for other snapshots, see Supplementary Fig. S10.

fluoride ions do not locate at the top of the valence band, but rather at its bottom. The strong narrowing of the band gap is therefore due to the different structure of the material. In a previous study on TiO_2 nanocrystals, Chen *et al.* have shown that, due to the presence of structural disorder, their materials exhibit a band gap substantially smaller than the one of pure bulk materials [46]. It is very likely that similar effects are at play here.
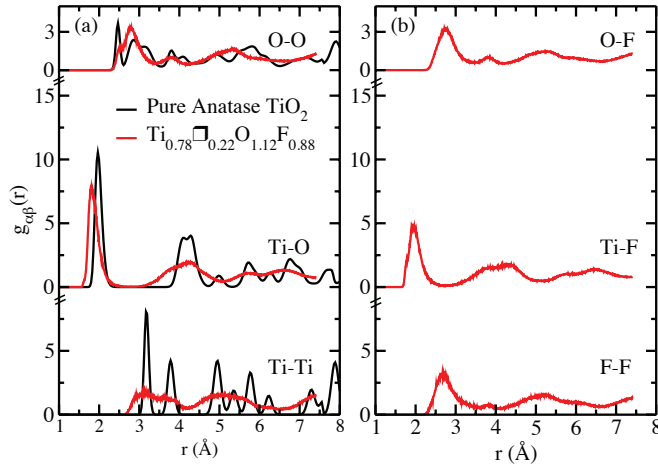
Figure 5. Radial distribution functions. Partial radial distribution functions $g_{\alpha\beta}(r)$ at ambient conditions calculated from a classical MD simulation of pure TiO_2 anatase (black) and from a DFT-based simulation of the configuration selected by the screening procedure (red).

The structural disorder is apparently at the origin of these strong electronic structure changes. To test this

idea, in Fig. 5 we show the partial radial distribution functions at ambient conditions $g_{\alpha\beta}(r)$ for the simulated pure anatase TiO_2 and for the fluorinated anatase configuration selected by the screening procedure. The effect of the disorder introduced by the vacancies is immediately evident looking at the $g_{Ti-Ti}(r)$ and at the $g_{O-O}(r)$. The $g_{Ti-O}(r)$ structure seems to be conserved to a large extent at least for the first two shells, although the presence of vacancies induces a shortening of the first neighbour distance. The effect of disorder is also clear when looking for example at the region in between the first two peaks. We also observe that on the one hand, $g_{Ti-O}(r)$ and $g_{Ti-F}(r)$ are very similar, and so are the $g_{O-O}(r)$, $g_{F-F}(r)$ and $g_{O-F}(r)$. This confirms that the fluorine atoms substitute the oxygen ones inside the anatase structure.

In conclusion, in order to characterise fluorinated anatase $Ti_{0.78}\square_{0.22}F_{0.88}O_{1.12}$, we have developed a screening procedure employing a polarisable force–field. It has allowed us (i) to select the best configurations starting from a very large pool (hundreds of thousands) of possible configurations; (ii) to reproduce the experimental structure, (iii) to study details of the partial atomic and electronic structure using DFT-based molecular dynamics. Our results show that fluorinated anatase has a highly disordered structure, which results in a lower band gap, by 0.8 eV, compared to conventional anatase. Therefore we conclude that fluorination appears as a very promising route for tuning material properties. This may be exploited for several applications, for example photocatalysis.

METHODS

We have performed the classical simulations using the software CP2K (single point calculations/geometry/cell optimisations, i.e., steps 1) to 3) of the screening procedure) and the in-house simulation software PIMAIM (molecular dynamics simulations, step 4) and 5) of the screening procedure). We have cut off the short–range interactions at half the norm of the shortest box vector (or less in NPT runs). The time step for the integration of the equations of motion has been set to 1 fs.

The DFT-based MD simulation has also been performed using the software CP2K [47], using the Quickstep algorithm. We have used the GGA PBE [48] exchange-correlation functional and we have employed the DZVP-MOLOPT-SR-GTH basis set [49]. Moreover, we have used the Goedecker-Teter-Hutter [50] pseudopotentials; for Ti atoms, the electronic orbitals explicitly represented are $3s^23p^63d^24s^2$, for O atoms $2s^22p^4$ and for F atoms $2s^22p^5$. We have set a plane wave cut-off of 400 Ry. We have added dispersive interactions through the use of the DFT-D3 correction [51], with a cutoff radius of 30 Å. We have accumulated the trajectory for 10 ps, with the simulations time step being 0.5 fs. We have conducted the simulation in the NVT ensemble with a

target temperature of 300 K. We have calculated the electronic density of states on a series of snapshot extracted from the trajectory, using the HSE06 functional [42, 43].

[1] Chen, X. & Mao, S. S. Titanium Dioxide Nanomaterials: Synthesis, Properties, Modification and Applications. *Chem. Rev.* **107**, 2891–2959 (2007).

[2] Kavan, L., Grätzel, M., Gilbert, S. E., Klemenz, C. & Scheel, H. J. Electrochemical and Photoelectrochemical Investigation of Single–Crystal anatase. *J. Am. Chem. Soc.* **118**, 6716–6723 (1996).

[3] O'Regan, B. & Grätzel, M. A Low–Cost, High–Efficiency Solar Cell Based on Dye-Sensitized Colloidal TiO_2 Films. *Nature* **353**, 737–740 (1991).

[4] Fujishima, A. & Honda, K. Electrochemical Photolysis of Water at a Semiconductor Electrode. *Nature* **238**, 37–38 (1972).

[5] Hoffmann, M. R., Martin, S. T., Choi, W. & Bahnemann, D. W. Environmental Applications of Semiconductor Photocatalysis. *Chem. Rev.* **95**, 69–96 (1995).

[6] Kudo, A. & Miseki, Y. Heterogeneous Photocatalyst Materials for Water Splitting. *Chem. Soc. Rev.* **38**, 253–278 (2008).

[7] Ravelli, D., Dondi, D.,Fagnoni, M. & Albini, A. Photocatalysis. A Multi–Faceted Concept for Green Chemistry. *Chem. Soc. Rev.* **38**, 1999–2011 (2009).

[8] Kamat, P. V. TiO_2 Nanostructures: Recent Physical Chemistry Advances. *J. Phys. Chem. C* **116**, 11849–11851 (2012).

[9] Wagemaker, M., Borghols, W. J. H. & Mulder, F. M. Large Impact of Particle Size on Insertion Reactions. A Case for Anatase Li_xTiO_2. *J. Am. Chem. Soc.* **129**, 4323–4327 (2007).

[10] Yang, M.-C., Lee, Y.-Y., Xu, B., Powers, K. & Meng, Y. S. TiO_2 Flakes as Anode Materials for Li–Ion–Batteries. *J. Power Sources* **207**, 166–172 (2012).

[11] Morgan, B. J. & Watson, G. W. Role of Lithium Ordering in the Li_xTiO_2 Anatase $\rightarrow$ Titanate Phase Transition. *J. Phys. Chem. Lett.* **2**, 1657–1661 (2011).

[12] Yildirim, H., Greeley, J. P. & Sankaranarayanan, S. K. R. S. Concentration–Dependent Ordering of Lithiated Amorphous TiO_2. *J. Phys. Chem. C* **117**, 3834–3845 (2013).

[13] Morgan, B. J. & Madden, P. A. Lithium Intercalation into TiO_2(B): A Comparison of LDA, GGA, and GGA+U Density Functional Calculations. *Phys. Rev. B* **86**, 035147/1–035147/13 (2012).

[14] Morgan, B. J. & Watson, G. W. GGA+U Description of Lithium Intercalation into Anatase TiO_2. *Phys. Rev. B* **82**, 144119/1–144119/11 (2010).

[15] Tosoni, S., Lamiel-Garcia, O., Hevia, D. F. & Illas, F. Theoretical Study of Atomic Fluorine Diffusion through Bulk TiO_2 Polymorphs. *J. Phys. Chem. C* **117**, 5855–5860 (2013).

[16] Tosoni, S., Lamiel-Garcia, O., Hevia, D. F., Miguel, J. & Illas, F. Electronic Structure of F-doped Bulk Rutile, Anatase, and Brookite Polymorphs of TiO_2. *J. Phys. Chem. C* **116**, 12738–12746 (2012).

[17] Samadpour, M. *et al.* Fluorine Treatment of TiO_2 for Enhancing Quantum Dot Sensitized Solar Cell Performance. *J. Phys. Chem. C* **115**, 14400–14407 (2011).

[18] Czoska, A. M. *et al.* The Nature of Defects in Fluorine–Doped TiO_2. *J. Phys. Chem. C* **112**, 8951–8956 (2008).

[19] Wang, Y. *et al.* A Selective Etching Phenomenon on {001} Faceted Anatase Titanium Dioxide Single Crystal Surfaces by Hydrofluoric Acid. *Chem. Commun.* **47**, 2829–2831 (2001).

[20] Wang, Y. *et al.* Nature of Visible–Light Responsive Fluorinated Titanium Dioxides. *J. Mater. Chem. A* **1**, 12948–12953 (2013).

[21] Yang, H. G. *et al.* Anatase TiO_2 Single Crystals with a Large Percentage of Reactive Facets. *Nature* **453**, 638–641 (2008).

[22] Yang, S. & Halliburton, L. E. Fluorine Donors and Ti^{3+} Ions in TiO_2 Crystals. *Phys. Rev. B* **81**, 035204/1–035204/7 (2010).

[23] Li, W. *et al.* High Substitution Rate in TiO_2 Anatase Nanoparticles with Cationic Vacancies for Fast Lithium Storage. Under review (2015).

[24] Curtarolo, S. *et al.* The High–Throughput Highway to Computational Materials Design. *Nat. Mater.* **12**, 191–201 (2013).

[25] Zakutayev, A. *et al.* Theoretical Prediction and Experimental Realization of New Stable Inorganic Materials Using the Inverse Design Approach. *J. Am. Chem. Soc.* **135**, 10048–10054 (2013).

[26] Rondinelli, J. M. *et al.* Accelerating Functional Materials Discovery. *Am. Ceram. Soc. Bull.* **92**, 14–21 (2013).

[27] Catlow, C. R. A., Freeman, C. M. & Royle, R. L. Recent Studies Using Static Simulation Techniques. *Physica B* **131**, 1–12 (1985).

[28] Catlow, C. R. A. & James, R. Disorder in TiO_{2-x}. *Proc. R. Soc. Lond. A* **384**, 157–173 (1982).

[29] Mostoller, M. & Wang, J. C. Ionic Potential Models in Insulators Having the Rutile Structure. *Phys. Rev. B* **32**, 6773–6786 (1985).

[30] Matsui, M. & Akaogi, M. Molecular Dynamics Simulation of the Structural and Physical Properties of the Four Polymorphs of TiO_2. *Mol. Simulat.* **6**, 239–244 (1991).

[31] Sawatari, H., Iguchi, E. & Tilley, R. Formation Energies of Point Defects in Rutile TiO_2. *J. Phys. Chem. Solids* **43**, 1147–1155 (1982).

[32] Post, J. E. & Burnham, C. W. Ionic Modeling of Mineral Structures and Energies in the Electron Gas Approximation: TiO_2 Polymorphs, Quartz Forsterite, Diopside. *Amer. Miner.* **71**, 142–150 (1986).

[33] Han, X. J. *et al.* Polarizable Interatomic Force Field for TiO_2 Parametrized Using Density Functional Theory. *Phys. Rev. B* **81**, 134108/1–134108/9 (2010).

[34] Corradini, D., Ishii, Y., Ohtori, N. & Salanne, M. DFT–based polarizable force field for TiO_2 and SiO_2. *Model. Simul. Mater. Sci. Eng.* **xx**, xxxx-xxxx (2015).

[35] Salanne, M. *et al.* Including Many–Body Effects in Models for Ionic Liquids. *Theor. Chem. Acc.* **131**, 1143/1–1143/16 (2012).

[36] Tazi, S. *et al.* A Transferable Ab Initio Based Force Field for Aqueous Ions. *J. Chem. Phys.* **136**, 114507/1–114507/12 (2012).

[37] Wilmer, C. E. *et al.* Large–Scale Screening of Hypothetical Metal–Organic Frameworks. *Nat. Chem.* **4**, 83–89 (2012).

[38] Coudert, F.-X. Systematic Investigation of the Mechanical Properties of Pure Silica Zeolites: Stiffness, Anisotropy, and Negative Linear Compressibility. *Phys. Chem. Chem. Phys.* **15**, 16012–16018 (2013).

[39] Horn, M., Schwerdtfeger, C. F. & Meagher, E. P. Refinement of the Structure of Anatase at Several Temperatures. *Z. Kristallogr.* **136**, 273–281 (1972).

[40] Hemmati, M., Wilson, M. & Madden, P. A. Structure of Liquid Al_2O_3 from a Computer Simulation Model. *J. Phys. Chem. B* **103**, 4023–4028 (1999).

[41] Wilson, A. J. C. editor, *International Tables for X-Ray Crystallography* (Kluwer Academic Publisher, Dordrecht, 1992).

[42] Heyd, J., Scuseria, G. E & Ernzerhof, M. Hybrid Functionals Based on a Screened Coulomb Potential. *J. Chem. Phys.* **118**, 8207–8215 (2003).

[43] Heyd, J., Scuseria, G. E. & Ernzerhof, M. Erratum: "Hybrid Functionals Based on a Screened Coulomb Potential" [J. Chem. Phys. 118, 8207 (2003)]. *J. Chem. Phys.* **124**, 219906 (2006).

[44] Scanlon, D. O. *et al.* Band Alignment of Rutile and Anatase TiO_2. *Nat. Mater.* **12**, 798–801 (2013).

[45] Harb, M., Sautet, P. & Raybaud, P. Origin of the Enhanced Visible-Light Absorption in N-Doped Bulk Anatase TiO_2 from First-Principles Calculations. *J. Phys. Chem. C* **115**, 19394–19404 (2011).

[46] Chen, X., Liu, L., Yu, P. Y. & Mao, S. S. Increasing Solar Absorption for Photocatalysis with Black Hydrogenated Titanium Dioxide Nanocrystals. *Science* **331**, 746–750 (2011).

[47] VandeVondele, J. *et al.* QUICKSTEP: Fast and accurate density functional calculations using a mixed Gaussian and plane waves. *Comp. Phys. Commun.* **167**, 103–128 (2005).

[48] Perdew, J. P., Burke, K. & Ernzerhof, M. Generalized gradient approximation made simple. *Phys. Rev. Lett.* **77**, 3865–3868 (1996).

[49] VandeVondele, J. & Hutter, J. Gaussian basis sets for accurate calculations on molecular systems in gas and condensed phases. *J. Chem. Phys.* **127**, 114105/1–114105/9 (2007).

[50] Goedecker, S., Teter, M. & Hutter, J. Separable dual-space Gaussian pseudopotentials. *Phys. Rev. B* **54**, 1703–1710 (1996).

[51] Grimme, S., Antony, J., Ehrlich, S. & Krieg, H. A consistent and Accurate Ab Initio Parametrization of Density Functional Dispersion Correction (DFT-D) for the 94 Elements H-Pu. *J. Chem. Phys.* **132**, 154104/1–154104/19 (2010).

[52] Burbano, M., Nadin, S., Marrocchelli, D., Salanne M. & Watson, G. W. Ceria Co–doping: Synergistic or Average Effect? *Phys. Chem. Chem. Phys.* **16**, 8230–8331 (2014).

[53] Marrocchelli, D., Madden, P. A., Norberg, S. T. & Hull, S. Structural Disorder in Doped Zirconias, Part II: Vacancy Ordering Effects and the Conductivity Maximum. *Chem. Mater.* **23**, 1365–1373 (2011).

ACKNOWLEDGEMENTS

AUTHOR CONTRIBUTIONS

D.C. and M.S. have designed research. D.C. has implemented the screening procedure and has performed most of the simulations. M.S. has conducted the band gap calculations. D.C. and M.S. have written the manuscript and prepared the figures. D.D. has provided the experimental input. All the authors have participated in the discussions and reviewed the manuscript.

SUPPLEMENTARY INFORMATION

In Supplementary Section S1, we describe the analytic form of the classical force–field employed to perform the classical MD simulations and we tabulate its parameters (see Supplementary Tables S1 and S2). In Supplementary Section S2, we compare the results reproduced by our classical force–field to DFT–calculated quantities. We first compare the results for the relative stability of structures containing only one vacancy and differing by the positioning of the F atoms (see Supplementary Fig. S6). Then we compute the DFT–energies (before and after relaxation) of the structures found by our screening procedure and we compare them to the DFT–energies of an equal number of structures selected at random from the pool of starting configurations (see Supplementary Fig. S7). Supplementary Section 3 deals with the energy distributions at the different screening steps. Fig. S8 shows the distribution of the energies of the configurations tested and retained at steps 1) to 4) of the screening procedure and Fig. S9 provides the positions of all the atoms along the DFT–based MD simulation. In Supplementary Section 4, the density of state for 10 different configurations extracted from this trajectory are shown in Fig. S10. Finally, an example CP2K input is provided in Supplementary Section S5.

S1. CLASSICAL MODEL

We describe the interaction potential between the ions by a classical polarisable force–field whose parameters we derive from *ab initio* DFT simulations. Details on how to extract the parameters of the classical force–field from DFT simulations are reported in earlier works (see Ref. [34–36] in the main text). In particular, the detailed procedure used for the pure phases of TiO_2 together with its validation are reported in Ref. [34] (of the main text) and are not repeated here. The force–field parameters for the fluoride ions are obtained in an analogous fashion. We do report here in the following the analytic form of the classical force–field that we use, together with its parameters.

A. Polarisable ion model (PIM)

The repulsive and dispersive terms of the interactions are taken into account using the the Born–Mayer–Huggins (BMH) form of the interaction potential:

$$V_{\mathrm{BMHFTD}} = \sum_{i,j>i} A_{ij} e^{-B_{ij}r_{ij}} - f_6^{ij}(r_{ij}) \frac{C_6^{ij}}{r_{ij}^6}$$
$$- f_8^{ij}(r_{ij}) \frac{C_8^{ij}}{r_{ij}^8} . \qquad (S5)$$

The damping functions are Tang-Toennies functions of the form

$$f_n^{ij}(r_{ij}) = 1 - e^{b_D^{ij}r_{ij}} \sum_{k=0}^{n} \frac{(b_D^{ij}r_{ij})^k}{k!} . \qquad (S6)$$

When performing molecular dynamics simulations, we add a Gaussian term in the Ti–O and Ti–F interactions that acts as a steep repulsive wall and accounts for the oxide/fluoride anion hard core:

$$V_{\mathrm{Gaussian}} = \sum_{i\in O,F,j\in Ti} B_{ij} e^{-d_{ij}r_{ij}^2} . \qquad (S7)$$

This extra term is used in cases where the ions are strongly polarised to avoid instability problems at very small anion–cation separations.

For the Coulombic part of the interaction potential,

$$V_{\mathrm{Coulomb}} = \sum_{i,j>i} \frac{q_i q_j}{r_{ij}} , \qquad (S8)$$

the formal charges for the ionic species are used, $-2e$ for O ions, $-e$ for F ions and $+4e$ for Ti ions. The many–body electrostatic interactions are described by the induced dipoles $\boldsymbol{\mu}_i$, obtained at each MD step minimising the polarisation energy

$$V_{\mathrm{pol}} = \sum_i \frac{1}{2\alpha_i}|\boldsymbol{\mu}_i|^2 + \sum_{i,j>i} \left[\left(q^i \mu_\alpha^j g^{ij}(r_{ij}) - q^j \mu_\alpha^i g^{ji}(r_{ij}) \right) \right.$$
$$\left. T_{ij}^\alpha - \mu_\alpha^i \mu_\beta^j T_{ij}^{\alpha\beta} \right] \qquad (S9)$$

where the Einstein summation convention is assumed, α_i is the atomic polarisability and T are the multipole interaction tensors. The damping function $g_{ij}(r_{ij})$ is of the Tang-Toennies form

$$g_{ij}(r_{ij}) = 1 - c_{ij} e^{-b_{ij}r_{ij}} \sum_{k=0}^{4} \frac{(b_{ij}r_{ij})^k}{k!} . \qquad (S10)$$

B. Parameterisation

The repulsion and polarisation parameters of the force–field have been fitted in order to reproduce the forces and dipoles extracted from DFT calculations, using a well-established procedure, see Ref. [34] in the main text. In the present case, we obtain final χ^2 values of 0.16 and 0.37 for the fits of dipoles and forces, respectively. Such values are similar to the ones obtained in our recent work on other oxide materials, i.e. rare earth doped ceria, for example [52]. The dispersion interactions are not taken into account in a proper way in the DFT calculations we have performed. The corresponding parameters have not been fitted, instead they have been taken from our previous works on fluorides and oxides, see Ref. [35] in the main text. Finally, the Gaussian term parameters have been chosen following Marrocchelli *et al.* [53]. The obtained parameters are reported in Table **S1** for the BMH part of the force–field and in Table **S2** for the polarisation part.

S2. COMPARISON BETWEEN AB INITIO AND CLASSICAL SIMULATIONS

We assess the behaviour of our force–field in the fluorinated samples, by comparing the results of classical and DFT calculations. For simplicity, we consider the case of one single fluorination, as in Ref. [23] in the main text. We consider here the system $Ti_{127}\square_1F_4O_{252}$ and we distribute the F atoms either at random positions in the lattice (where they substitute O atoms) or at positions neighbouring the cationic vacancy. The latter correspond to 2–coordinated F, i.e. $F-Ti_2\square_1$. We consider the cases where 0, 1, 2, 3 or 4 F are neighbouring the vacancy and have therefore a $F-Ti_2\square_1$ environment, with the remaining F having the $F-Ti_3$ environment. We compare the energy calculated in 0 K cell optimisations, using either DFT or our force field. The comparison for the energies is shown in Fig. **S6**. We see that our classic force-field is able to closely reproduce the decrease in energy with the

increase in the number of $F - Ti_2\square_1$, observed by DFT calculations (see also Ref. [23] in the main text).
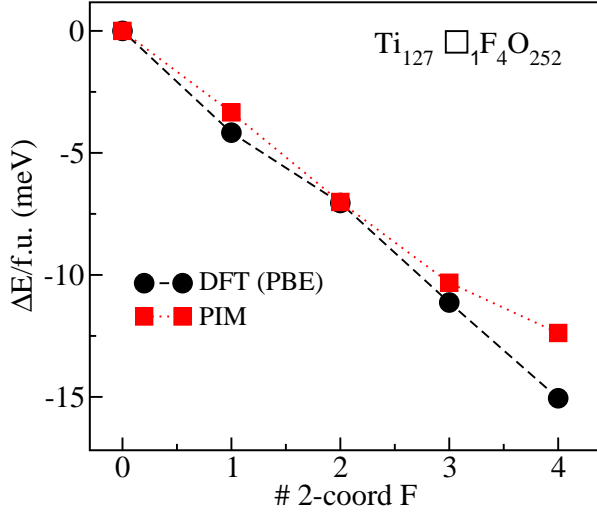
Figure S6. **Comparison between DFT and classical potential.** Difference in energy between the case where all F atoms in $Ti_{127}\square_1F_4O_{252}$ have environment $F - Ti_3$ and the cases where F is progressively added in positions neighbouring the vacancies and has thus $F - Ti_2\square_1$ environment. We have calculated this quantity by DFT (circles) and by our classic force–field (squares).

Finally in Fig. **S7** we show the comparison between the DFT energies of the configurations selected by the screening procedures and the same number of configurations taken at random from the initial pool of configurations of the $Ti_{100}\square_{28}F_{112}O_{144}$, before (panel a) and after (panel b) relaxation of the atomic positions and of the cell dimensions.
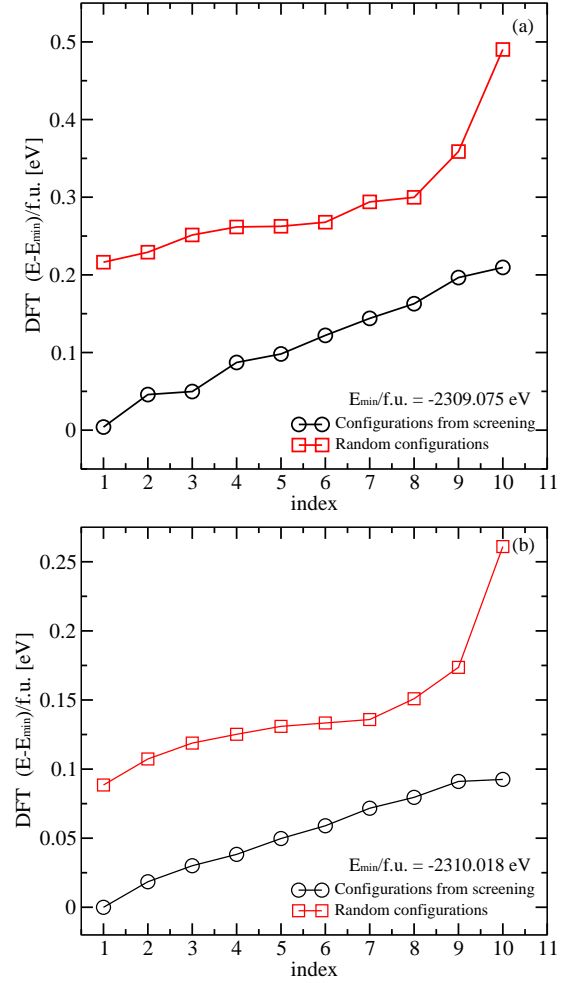
Figure S7. **DFT energies of the configurations selected by the screening.** For the configurations left at the end of the screening procedure, we take their initial structures and calculate their DFT energy (black circles) before (a) and after relaxation (b). Those are compared with the DFT energies of the same number of configurations taken at random (red squares) from the initial pools of configuration. The values of the energies are plotted relative to the lowest DFT energy configuration. Panel (a) shows the results obtained before the DFT relaxation, panel (b) shows the results obtained after the DFT relaxation.

Table S1. **BMH parameters.** Parameters of the BMH potential extracted from DFT simulations.

Atom Pair	A_{ij} (Ha)	a_{ij} (Å^{-1})	B_{ij} (Ha)	d_{ij} (Å^{-2})	C_6^{ij} (Ha Å^6)	C_8^{ij} (Ha Å^8)	b_D^{ij} (Å^{-1})
O–O	290.4	4.54668	–	–	0.48309	2.61949	2.64562
O–F	278.4	4.71487	–	–	0.39890	1.55438	3.11805
O–Ti	43.0	2.86431	50,000	6.4279	–	–	–
F–F	282.3	4.61849	–	–	0.32938	0.922357	3.59048
F–Ti	28.3	3.13082	50,000	6.4279	–	–	–
Ti–Ti	1.0	9.44863	–	–	–	–	–

Table S2. **Polarisation parameters.** Parameters of the polarisation part of the interaction potential extracted from DFT simulations.

Atom / Atom Pair	α (Å^3)	b_{ij} (Å^{-1})	c_{ij}
O	1.59150		
O–O		4.74888	2.227
O–F		–	–
O–Ti		3.90122	2.13327
F	1.16458		
F–O		–	–
F–F		–	–
F–Ti		4.16887	2.90678
Ti	0.20442		
Ti–O		3.90122	-1.90330
Ti–F		4.16887	-2.66057
Ti–Ti		–	–

S3.   SCREENING PROCEDURE
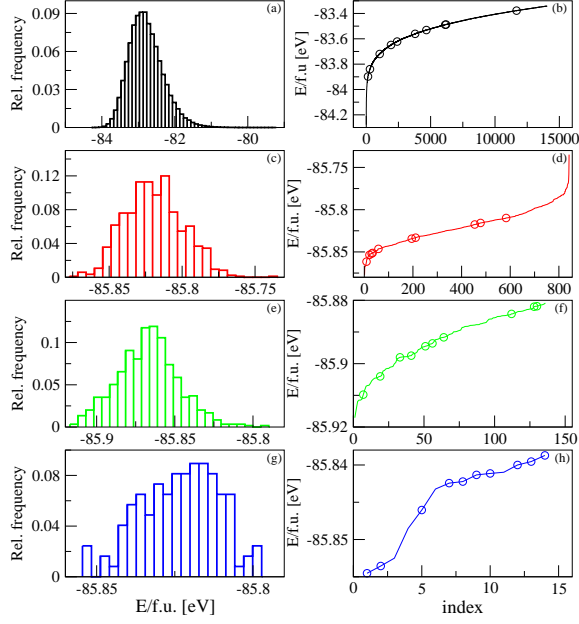
Figure S8. **Energy distributions at screening steps 1) to 4).**   The panels on the left show the relative frequency histograms of the energies calculated for all the configurations tested at each step, while the panels on the right show the sorted energies of the configurations retained after each step. The energies shown are: (a,b) at 0 K for the starting unrelaxed structures; (c,d) at 0 K after the optimization of the atomic positions; (e,f) at 0 K after the optimization of the atomic positions and cell vector lengths; (g,h) at 300 K after the tempering from 25 to 300 K. The open circles in panels (b,d,f,h) indicate the energy of the configurations left at the end of the screening procedure at each previous step. Note that the number of retained configurations can be less than the target one (see main text). This is due to "crashed" unstable configurations that are eliminated from the pool.
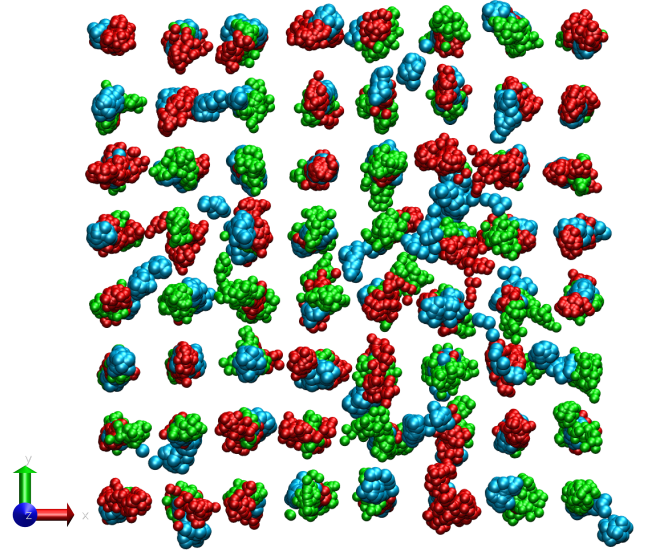
Figure S9. **Positions of the atoms along the DFT–based MD simulation.**   The positions of the Ti (blue), O (red) and F (green) atoms are shown every 10 steps of the simulation. Although structural relaxation close to the vacancies is observed, there is no major lattice rearrangement.

S4. TI$_{0.78}\square_{0.22}$O$_{1.12}$F$_{0.88}$ DENSITY OF STATES
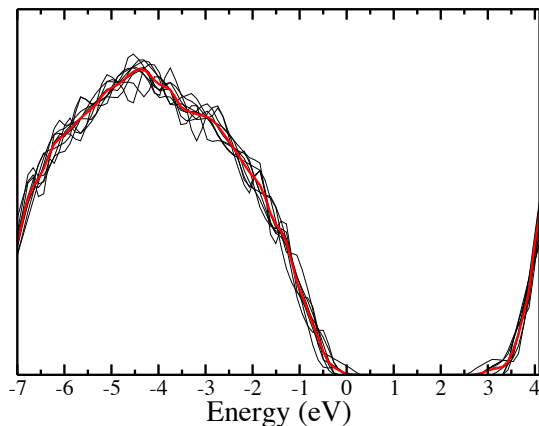
Figure S10. **Density of states for several Ti$_{0.78}\square_{0.22}$O$_{1.12}$F$_{0.88}$ configurations.** The density of states has been calculated for 10 configurations extracted from the DFT–based molecular dynamics trajectory. The results are shown as thin black lines while their average is shown using a thick red line.

S5. CP2K INPUT FILE

We here report an example of CP2K input file, prepared for running the system Ti$_{127}\square_1$F$_4$O$_{252}$ in the NVT ensemble at $T = 300$ K, using our classical force–field.

```
&GLOBAL
  PROJECT 1fn-loc-npt
  RUN_TYPE MD
  PRINT_LEVEL LOW
  WALLTIME 50000
  &PRINT
    &EACH
      MD 500
    &END EACH
  &END PRINT
&END GLOBAL

&MOTION
  &MD
    &THERMOSTAT
      &NOSE
        LENGTH 3
        YOSHIDA 3
        TIMECON 1000.0
        MTS 2
      &END NOSE
    &END THERMOSTAT
    ENSEMBLE NVT
    STEPS 100000
    TIMESTEP 1
    TEMPERATURE 300.0
    &PRINT
      &PROGRAM_RUN_INFO
        &EACH
          MD 500
        &END EACH
      &END PROGRAM_RUN_INFO
      &ENERGY
        &EACH
          MD 500
        &END EACH
      &END ENERGY
    &END PRINT
  &END MD

  &PRINT
    &TRAJECTORY
      &EACH
        MD 5000
      &END EACH
```

```
      &END TRAJECTORY
      &RESTART_HISTORY
        &EACH
          MD 10000
        &END EACH
      &END RESTART_HISTORY
      &RESTART
        BACKUP_COPIES 1
      &END RESTART
    &END PRINT

&END MOTION

&FORCE_EVAL
  METHOD FIST
  &MM
    &FORCEFIELD
      &SPLINE
        EMAX_SPLINE 8.0
        RCUT_NB 7.541
      &END SPLINE
      &NONBONDED
        &BMHFTD
          atoms O O
          A 290.4
          B 4.54668
          C 0.483092
          D 2.61949
          BD 2.64562
        &END BMHFTD
        &BMHFTD
          atoms O F
          A 278.4
          B 4.71487
          C 0.3989
          D 1.55438
          BD 3.11805
        &END BMHFTD
        &BMHFTD
          atoms O Ti
          A 43.0004
          B 2.86431
          C 0.0
          D 0.0
          BD 0.0
        &END BMHFTD
        &BMHFTD
          atoms F F
          A 282.3
          B 4.61849
          C 0.32938
          D 0.922357
          BD 3.59048
        &END BMHFTD
        &BMHFTD
          atoms F Ti
          A 28.3129
          B 3.13082
          C 0.0
          D 0.0
          BD 0.0
        &END BMHFTD
        &BMHFTD
          atoms Ti Ti
          A 1.0
          B 9.44863
          C 0.0
          D 0.0
          BD 0.0
        &END BMHFTD
      &END NONBONDED
      &CHARGE
        atom O
        CHARGE -2.0000
      &END CHARGE
      &CHARGE
        atom F
        CHARGE -1.000
      &END CHARGE
      &CHARGE
        atom Ti
        CHARGE 4.000
      &END CHARGE
      &DIPOLE
        atom O
        APOL 1.59150
        &DAMPING
          TYPE Tang-Toennies
          ATOM O
          BIJ 4.74888
          ORDER 4
          CIJ 2.227
        &END DAMPING
        &DAMPING
          TYPE Tang-Toennies
          ATOM F
          BIJ 0.0
          ORDER 4
          CIJ 0.0
        &END DAMPING
        &DAMPING
          TYPE Tang-Toennies
          ATOM Ti
          BIJ 3.90122
          ORDER 4
          CIJ 2.13327
        &END DAMPING
      &END DIPOLE
      &DIPOLE
        atom F
        APOL 1.16458
        &DAMPING
          TYPE Tang-Toennies
          ATOM O
          BIJ 0.0
          ORDER 4
          CIJ 0.0
        &END DAMPING
        &DAMPING
          TYPE Tang-Toennies
          ATOM F
          BIJ 0.0
          ORDER 4
          CIJ 0.0
        &END DAMPING
        &DAMPING
          TYPE Tang-Toennies
          ATOM Ti
          BIJ 4.16887
          ORDER 4
          CIJ 2.90678
        &END DAMPING
      &END DIPOLE
      &DIPOLE
        atom Ti
        APOL 0.20442
        &DAMPING
          TYPE Tang-Toennies
```

```
      ATOM O
      BIJ 3.90122
      ORDER 4
      CIJ -1.90330
    &END DAMPING
    &DAMPING
      TYPE Tang-Toennies
      ATOM F
      BIJ 4.16887
      ORDER 4
      CIJ -2.66057
    &END DAMPING
    &DAMPING
      TYPE Tang-Toennies
      ATOM Ti
      BIJ 0.0
      ORDER 4
      CIJ 0.0
    &END DAMPING
    &END DIPOLE
  &END FORCEFIELD
  &POISSON
    &EWALD
      EWALD_TYPE EWALD
      EWALD_ACCURACY 1.0e-6
      ALPHA 0.39297
      RCUT 7.541
      GMAX  19
      O_SPLINE 6
      &MULTIPOLES T
        MAX_MULTIPOLE_EXPANSION DIPOLE
        POL_SCF CONJUGATE_GRADIENT
        EPS_POL 1.0e-6
        MAX_IPOL_ITER 100
      &END MULTIPOLES
    &END EWALD
  &END POISSON
  &PRINT
    &ITER_INFO
      &EACH
        MD 500
      &END EACH
    &END ITER_INFO
  &END PRINT
  &END MM
  &SUBSYS
    &CELL
      ABC 15.082   15.100   20.431
      PERIODIC XYZ
    &END CELL
    &COORD
Ti     0.0092526897      2.8105961256      1.2817567910
Ti     0.0506441050      2.8142375601     11.4965161278
Ti     0.0373622332      6.5721801714      1.2709321758
Ti     0.0686762730      6.5665219023     11.4946324231
Ti     0.0562138844     10.3752296101      1.2665654437
Ti     0.0930430310     10.3904422990     11.4782100093
Ti     0.0549241715     14.1400567348      1.2665611962
Ti     0.0936365683     14.1524822380     11.5041248161
Ti     3.7759452413      2.7912937424      1.2688107899
Ti     3.8063797628      2.7956146571     11.4642638441
Ti     3.8078281440      6.6046747939      1.2696113779
Ti     3.8492414420      6.6184808818      1.4971070498
Ti     3.7974199211     10.3708698515      1.2688784727
Ti     4.0203828276     10.3677305287     11.5495142728
Ti     3.8655421361     14.1362671796      1.2900093286
Ti     3.9310964920     14.1262510213     11.5145891174
Ti     7.5491134334      2.8313499507      1.2719267327
Ti     7.5681863082      2.8382965342     11.4772300865
Ti     7.5368925139      6.5978464134      1.2781345496
Ti     7.5546748184      6.6174658832     11.5111042655
Ti     7.6040157639     10.3627061247      1.2805033765
Ti     7.4622388553     10.3668239102     11.5501643194
Ti     7.6175012880     14.1114312193      1.2650385392
Ti     7.6209604718     14.1130553468     11.4186707741
Ti    11.2875516032      2.8265300096      1.2750800406
Ti    11.3235793462      2.8352807892     11.5014763035
Ti    11.3484903199      6.5950075403      1.2739718867
Ti    11.3781032837      6.6029488983     11.4994060714
Ti    11.3726570777     10.3438744021      1.2627720004
Ti    11.3869501154     10.3461423554     11.4690935325
Ti    11.3948366064     14.1469191252      1.2706971376
Ti    11.4054648836     14.1624354118     11.5083237067
Ti     1.8955489882      0.9119266960      6.3887525432
Ti     1.8978237343      0.9133769789     16.5865526041
Ti     1.9257135506      4.6895911922      6.3785533854
Ti     1.9404118027      4.7089906429     16.6043602590
Ti     1.9343509155      4.8920662432      6.3790619262
Ti     1.9518346955      8.4999711634     16.5905279568
Ti     1.9525165596     12.2628886292      6.3944507948
Ti     1.9926244726     12.2501341949     16.5875104054
Ti     5.6656627583      0.9131930570      6.3865663437
Ti     5.6901942967      0.9481698804      6.6330334148
Ti     5.6745443041      4.7141749439      6.3817441594
Ti     5.6728571349      4.7060333573     16.6151178373
Ti     5.6902441722      8.4904488086      6.9882843939
Ti     5.7153330731      8.6525556067     16.5414092347
Ti     5.7379715177     12.2412941842      6.3973018808
Ti     5.7423884378     12.0693642357     16.5737394374
Ti     9.4163802659      0.9350747908      6.3775979904
Ti     9.4189961791      0.9328323469     16.5879520691
Ti     9.4321743134      4.7199806153      6.3924056704
Ti     9.4612587123      4.7409793512     16.5808044328
Ti     9.4762792944      8.4699692502      6.3887627110
Ti     9.4708341809      8.4964066142     16.5917323933
Ti     9.5120319609     12.2363807806      6.3787708348
Ti     9.5229186076     12.2437664886     16.6039733162
Ti    13.1755604919      0.9384609463      6.3897285094
Ti    13.1948430181      0.9502852356     16.5943500922
Ti    13.2282803150      4.6947621385      6.3859403535
Ti    13.2413926828      4.7075475043     16.5935058981
Ti    13.2653352736      8.4621554862      6.3840386973
Ti    13.2856875386      8.4838322335     16.6183482562
Ti    13.2613652772     12.2639923032      6.3832808596
Ti    13.2723944261     12.2572329389     16.6016691772
Ti     1.8726842508      2.8277145271      3.8381380587
Ti     1.9277061239      2.8560282353     14.0457425718
Ti     1.9037779579      3.8219888884      3.8299885073
Ti     1.9500277893      5.5995357070     14.0377142884
Ti     1.9505542997     10.3542152293      3.8309291523
Ti     1.9188210756     10.3586744344     13.9999692258
Ti     1.9606396537     14.1244640472      3.8294548938
Ti     2.0081827508     14.1401083529     14.0407335203
Ti     5.6451516258      2.8211456330      3.8251639215
Ti     5.6771534617      2.8233289488     14.0137900642
Ti     5.6939306575      6.5802023077      3.8398661875
Ti     5.7110707339      6.5163565261     14.0922412885
Ti     5.7065685497     10.3536592289      3.8328950365
Ti     5.7259910744     10.3529049623      3.8440195023
Ti     5.7839305475     14.2502023809     14.1071208952
Ti     9.4414783466      2.8054100029      3.8378804521
Ti     9.4601022918      2.8089565560     14.0435886792
Ti     9.4559310186      6.5808125184      3.8289539910
Ti     9.4828400504      6.6110676822     14.0401584228
Ti     9.4686206627     10.3787434428      3.8322819245
Ti     9.5764227300     10.3957776869     14.0042592707
Ti     9.4902917028     14.1449715650      3.8183244626
Ti     9.4994241638     14.1413719375     14.0343092357
```

```
Ti    13.1963868466      2.8028921853      3.8330370903
Ti    13.2349776080      2.8221974625     14.0457430133
Ti    13.2086296573      6.6062484093      3.8343715458
Ti    13.2553567868      6.6389670489     14.0553270443
Ti    13.2378534778     10.3725492480      3.8225087699
Ti    13.2727412239     10.3668247532     14.0490364628
Ti    13.2906480096     14.1262907986      3.8330226768
Ti    13.3149589939     14.1295796332     14.0592257214
Ti     0.0066710895      0.9204443731      8.9458796274
Ti     0.0148939416      0.8884050857     19.1569922011
Ti     0.0146594993      4.7197127478      8.9348798870
Ti     0.0132231931      4.6775070873     19.1563708286
Ti     0.0563794362      8.4793616509      8.9467179417
Ti     0.0637985346      8.4539855050     19.1521334552
Ti     0.0916563818     12.2514170022      8.9407169729
Ti     0.1158856593     12.2076921920     19.1291048606
Ti     3.7571423911      0.9333130434      8.9444795369
Ti     3.7586866054      0.8918372625     19.1586663416
Ti     3.7926965165      4.7202860335      8.9412286575
Ti     3.7920555593      4.6847533794     19.1618026706
Ti     3.8300050868      8.4805561564      8.9489178190
Ti     3.8666398983      8.4446081290     19.1350288637
Ti     3.8563427476     12.2313301734      8.9646627837
Ti     3.8768278425     12.2209716162     19.1602455252
Ti     7.5392813905      0.9386460067      8.9420091757
Ti     7.5556550309      0.9134362883     19.1636505061
Ti     7.5790224083      4.6986300311      8.9448911231
Ti     7.6067245098      4.6715777567     19.1394764767
Ti     7.6009694465      4.8881799553      8.9637637357
Ti     7.5831857750      8.4347571603     19.1551848208
Ti     7.6135486507     12.2488057989      8.9443334140
Ti     7.5865924905     12.2105094200     19.1472655490
Ti    11.3219739946      0.9148709362      8.9449524578
Ti    11.3338759041      0.8891791944     19.1462302817
Ti    11.3445534617      4.6992552914      8.9490786321
Ti    11.3455342690      4.6627009070     19.1549642197
Ti    11.3512777468      8.4906821868      8.9325965141
Ti    11.3386061373      8.4538641732     19.1394901190
Ti    11.3794957527     12.2767041122      8.9438094645
Ti    11.3877843706     12.2362558094     19.1515724146
O     -0.0022869352      2.6967833227      3.3683648221
O      0.0529688632      2.7249890910     13.5872398290
O      0.0422433279      6.3627538345      3.3074707460
O      0.0739841164      6.3938759503     13.5275939796
O      0.0365554610     10.4888750817      3.2976670005
O      0.0701141064     10.6244989097     13.5694870377
O      0.0571622153     14.3604200491      3.3352859678
O      0.1043977842     14.2771270428     13.5746828553
O      3.7873698560      2.5819113948      3.3091705576
O      3.8091571201      2.5873946025     13.4996670200
O      3.8535913484      6.8938177594     13.5491807775
O      3.7995996168     10.5912409401      3.3357654102
O      3.8495392942     14.0203146696      3.3664805956
O      3.9398325710     13.9984399455     13.5880148648
O      7.5257450105      2.9358544584      3.2996974804
O      7.5714144631      3.0433099259     13.5023921988
O      7.5446236283      8.8164491877      3.3322298826
O      7.5521620344      6.8133286564     13.5581050817
O      7.5914806394     10.2535920680      3.3683201023
O      7.6326650070     13.9012727510      3.3109861963
O      7.6237561579     13.8264265202     13.5524590663
O     11.2992642410      3.0458418563      3.3373461330
O     11.3280281078      3.0314286238     13.5614436989
O     11.3359339515      6.4736758110      3.3680000660
O     11.3784712743      6.6566926809     13.5868645454
O     11.3810010766     10.1291967456      3.3084725621
O     11.4172219207     10.0885366363     13.5767292037
O     11.3750520525     14.2608368682      3.2952312894
O     11.4035419985     14.2923327473     13.5282467896
O      1.8920111539      0.7573902469      8.4708043919
O      1.8922493525      0.6647126339     18.6939360765
O      1.9249082665      4.5021054974      8.4152607335
O      1.9352855834      4.4660779020     18.6278358412
O      1.9296354240      6.6733374780      8.4197987329
O      1.9510197607     12.4450806447      4.4688323143
O      1.9853979708     12.4425105425     18.6518300002
O      5.6687385718      6.7042755875      8.4206872613
O      5.6874875321      6.7341865795     18.6271776142
O      5.6721856466      4.8684856876      8.4116553863
O      5.6933290932      4.5546470328     18.6279847657
O      5.6882561274      8.6694080684      8.4519524378
O      5.7130218587      8.7617654367     18.6571104211
O      5.7420228025     12.1438583745      4.4725575174
O      7.5395390181     11.9181380627     18.6747228046
O      9.4165283996      1.0630004009      8.4088330583
O      9.4386433510      0.7794805591     18.6336511748
O      9.4357685623      4.9297616176      8.4529935230
O      9.4606020440      4.9415652150     18.6651012374
O      9.4820387407      8.3694106539     18.4832545793
O      9.4699704589      8.2631871171     18.6683678861
O      9.5175864541     12.0075432038      8.4275568685
O      9.5178748407     12.0639729860     18.6205482210
O     13.1778240075      1.1409470039      8.4561034154
O     13.1922204345      1.1189041253     18.6616416377
O     13.2303598457      4.5620960393      8.4738481055
O     13.2389368515      4.5015660723     18.8238313572
O     13.2875482430      8.2774671679      8.4251400025
O     13.2832231126      8.2435251580     18.6278012167
O     13.2590673501     12.3858653902      8.4136473865
O     13.2886850751     12.1549471037     18.6276477443
O      1.6792380075      2.8313579725      5.8897982264
O      1.7309968446      2.8588078968     16.0889854042
O      1.8568224364      5.5964538101      8.5543641611
O      1.8003852451      6.6165514370     16.0573277201
O      2.1791096721     10.3480364548      8.8618907043
O      2.1855366649     10.3603530656     16.1014918145
O      2.0840186270     11.1379506357      5.9279629747
O      1.8851929634     14.1341409634     16.1084868859
O      5.5928936186      2.8218726549      5.8570279479
O      5.5340524825      2.8357268602     16.0644138647
O      5.9359836220      6.5740143227      5.8613706564
O      5.9014987368      6.5289491195     16.0566550393
O      5.8202681560     10.3558548891      5.9307551705
O      5.7395600769     10.3694001153     16.0540031146
O      5.5223635933     14.1544765572      5.8948778047
O      5.6231123649     14.2494149034     16.0644610508
O      9.6738992345      2.7968536990      5.8597515173
O      9.6647191494      6.5985225931     16.0736590811
O      5.6838127398      5.5847536159      9.2720097788
O      9.6660883606      6.6269948919     16.1073127626
O      9.2775316233     10.3808227189      5.8909912300
O      9.3542821481     10.4022764574     16.1141004770
O      9.4255380934     14.1458365482      5.8534221408
O      9.3869736546     14.1542683026     16.0655712802
O     13.3044532291      2.8064294914      5.9205765521
O     13.3154024446      2.8327434087     16.1145121399
O     13.0040277946      6.6086201058      5.8928910307
O     13.0450667595      6.6316639614     16.1096598800
O     13.1335991063     10.3724764564      5.8632600280
O     13.5327422232     12.1203244950      5.8617411981
O     13.5404510326     14.1403696445     16.1015207395
O      0.0612417585      9.0088343860      8.0050433067
O      0.1179952991      0.9213077396     11.0392238481
O     -0.2287004771      4.7083932583      0.7871239191
O     -0.2033464162      4.7212868415     10.9895752919
O     -0.0152049761      8.4873793996      0.7404316193
O      0.0857049761      8.4788041005     10.9785000249
O      0.2576586752     12.2372615705      0.7511297707
```

```
 0     3.5038126666      0.9221370013      0.7898121285
 0     3.5459724319      0.9467618494     10.9782941314
 0     3.6138001775      4.7181584512      0.7405744675
 0     3.7912290205      4.7045336809     10.9524248071
 0     4.0034592404      8.4687117719      0.7523578725
 0     4.0710259509      8.4581308931     10.9991293777
 0     3.9296590838     12.2392499993      0.8017644026
 0     3.9725554175     12.2441637859     11.0937779572
 0     7.3912031098      0.9380251398      0.7416202509
 0     7.5782329020      0.9409593883     10.9499206183
 0     7.7435087642      4.7021350515      0.7583014693
 0     7.8163881164      4.6837477924     10.9548317485
 0     7.6293319436      8.4618365414      0.7979761483
 0     7.7190030393      8.4839371711     11.0855558375
 0     7.3477613461     12.2500754723      0.7845011408
 0     7.4061904199     12.2647493439     11.0241208925
 0    11.4730559807      0.9189041921      0.7590220624
 0    11.5608841968      0.9063877191     10.9723721028
 0    11.4119820011      4.6922973540      0.8010296263
 0    11.4668237730      4.7051515940     11.0411284425
 0    11.1038795762      8.4861548884      0.7808478547
 0    11.1316764255      8.4880955344     10.9937760214
 0    11.2120786149     12.2594068045      0.7391778996
 0    11.3844318714     12.2670116707     10.9770301498
 0     1.8638582388      3.0207547943      1.8050674229
 0     1.9010365279      3.0685385565     11.9929414075
 0     1.9021388031      6.7235187383      1.7275217999
 0     1.9635541048      6.6578129882     11.9821581615
 0     1.9428077732     10.1259712645      1.7715154664
 0     1.9669038199     10.1853083303     12.0344792446
 0     1.9621625649     14.0230583287      1.7991284932
 0     2.0189117945     14.1061649542     12.0391725703
 0     5.6430930598      2.9368537844      1.7215709314
 0     5.6870527180      2.8314538579     11.9336483065
 0     5.6851449437      6.3426539268      1.7732417658
 0     5.7129075600      6.3080940781     11.9825848845
 0     5.7041827906     10.2586187515      1.8004393975
 0     5.7465181589     10.2958040985     12.0423500082
 0     5.7161037780     14.3639895941      1.8068634268
 0     5.7724607436     14.4558033101     11.8853065225
 0     9.4332043265      2.5898290849      1.7752760936
 0     9.4778611738      2.5835242806     11.9899344039
 0     9.4512158144      6.4986543822      1.7962524164
 0     9.4835479522      6.4519581189     12.0375684511
 0     9.4569113089     10.5708993466      1.8051843773
 0     9.5304487961     10.5797895198     12.0429086017
 0     9.4867887531     14.2501072868      1.7229812289
 0     9.5052332402     14.2103288138     11.9852400998
 0    13.1939497223      2.7063452250      1.7978635099
 0    13.2385900913      2.7214324277     12.0263046857
 0    13.2001630346      6.8071779285      1.8040399620
 0    13.2490668278      6.8144202341     11.9975439615
 0    13.2357729435     10.4932981426      1.7239104605
 0    13.2789225949     10.3810186722     11.9833955591
 0    13.2817190643     13.8962747069      1.7704703815
 0    13.3185803989     13.9357820521     11.9997203983
 0     0.0023405852      0.8581098685      6.9160387112
 0     0.0240579712      0.9804197871     17.1264332075
 0     0.0073478564      4.9309257918      6.8979744431
 0     0.0191832455      4.9356287295     17.1215147197
 0     0.0524385114      8.5396942664      6.8526404597
 0     0.0711556613      8.6813144991     17.0861304843
 0     0.0927874617     12.0275570696      6.8926365997
 0     0.1152456606     12.0482733232     17.0720920509
 0     3.7530516096      1.1539528285      6.9005092670
 0     3.7430638043      1.1324672046     17.1355796631
 0     3.7929050168      4.7963548776      6.8443887482
 0     3.7977847291      4.9205939605     17.0907612704
 0     3.8284285266      8.2449403208      6.8865815510
 0     3.8739800521      8.3109047342     17.0419938547
 0     3.8490558712     12.1533916216      6.9238322625
 0     3.8899655575     12.3578151791     17.0930152252
 0     7.5352024976      1.0207445705      6.8462281539
 0     7.5627651276      1.1661932778     17.0883930382
 0     7.5796313527      4.4701244005      6.8816455903
 0     7.6080529942      4.5439394644     17.0783036239
 0     7.5991098634      8.4032184390      6.9208535462
 0     7.5923489915      8.4129783570     17.0883755764
 0     7.6081186258     12.4656181289      6.9044719295
 0     7.5842099803     12.4291414330     17.0965718833
 0    11.3240336491      0.6874900449      6.8811611803
 0    11.3338246086      0.7696910132     17.0674170087
 0    11.3406651648      4.6148385577      6.9170639229
 0    11.3573660406      4.6330058237     17.1178247849
 0    11.3469552369      8.7013974844      6.9067341178
 0    11.3517072387      8.7086211279     17.1315670131
 0    11.3785281080     12.3701449175      6.8513142558
 0    11.3956047390     12.4585169455     17.0805807392
 0     0.1434580193      2.8025228952      9.4640377960

 0     0.1798758842      2.7683636351     19.6894656064
 0     0.2565206371      6.5796710886      9.4208163149
 0     0.2494094097      6.5279760806     19.6587878817
 0    -0.1206131415     10.3804461429      9.4340652625
 0     0.1370774878     10.3271503935     19.6114941580
 0    -0.1365454287     14.1590236024      9.4680998144
 0    -0.1405125437     14.1082682127     19.6464468403
 0     3.9795163770      2.8006403770      9.4011406766
 0     3.9530496370      2.7479319430     19.6647668379
 0     3.6278635521      6.6180315224      9.4205598012
 0     3.9227780074      6.5588333695     19.6112743669
 0     3.6903855129     10.3861021241      9.4997885118
 0     3.5690634334     10.3410430819     19.6519069714
 0     3.9802308123     14.1060985019      9.4840154034
 0     4.0758771198     14.0910776698     19.6848128759
 0     7.3781064031      2.8295019896      9.3909574773
 0     7.6628207020      2.7872793291     19.6231218751
 0     7.3686832044      6.6324227358      9.4845319297
 0     7.3127576975      6.5670246964     19.6418908118
 0     7.6512528411     10.3523257589      9.4874769075
 0     7.8256626490     10.3192172788     19.6885123477
 0     7.8288570482     14.1077345453      9.4336171023
 0     7.7643342934     14.0692492105     19.6488186494
 0    11.1021390961      2.8372697854      9.4732389701
 0    11.0756176507      2.7910347174     19.6504400070
 0    11.4673951082      6.5825377083      9.4612822846
 0    11.5154069419      6.5513163465     19.6807877548
 0    11.5896097189     10.3531427697      9.4389267477
 0    11.5625911202     10.3050316987     19.6476935101
 0    11.2115830174     14.1511816635      9.4124177249
 0    11.4897468054     14.1047127765     19.6213503834
 0     1.9614642303      0.9112422076      4.3589691033
 0     2.0583346529      0.9260355534     14.5744588035
 0     2.1171507848      4.6867644277      4.3116423572
 0     2.2069284169      4.7162402547     14.5251470198
 0     1.7763225622      8.4885508888      4.2985514128
 0     1.8243166417      8.5125983122     14.5019385122
 0     1.7198074107     12.2692455597      4.3587443367
 0     2.0539369888     12.2504583122     14.5301958908
 0     5.8643664984      9.1057533275      4.3189518195
 0     5.9743794412      9.9785570114     14.4792728111
 0     5.5203160131      4.7122507946      4.2986798826
 0     5.4794681250      4.6918805469     14.4663591118
 0     5.4660110669      8.4961937608      4.3590362443
 0     5.8079483820     12.2391277396      4.3633165318
 0     9.2718660294      0.9360130984      4.2932103220
 0     9.2561294271      0.9427390090     14.5030036346
 0     9.2090334354      4.7230576019      4.3568309252
 0     9.2887428500      4.7482862558     14.5689233915

 0     9.5496161877      8.4655787066      4.3583869123
 0     9.3636141643      8.5170792067     14.5420130297
 0     9.7167654362     12.2359266140      4.3158399612
 0     9.7232058377     12.2472211924     14.5238623568
 0    12.9527206411      9.9411923475      4.3555941021
 0    13.0335437170      0.9500167173     14.5625100685
 0    13.3069160364      4.6938755115      4.3581284003
 0    13.3055255218      4.7258163708     14.5586923126
 0    13.4603063142      8.4641151104      4.3194203126
 0    13.5657530404      8.4853110445     14.5478680125
 0    13.1032510000     12.2600188022      4.3007815004
 0    13.1025482216     12.2761043908     14.5281475102
 0     0.3357565771     12.2484050849     10.9778758830
 0     1.9718724603      8.3542439861     18.6171564662
 0    13.1382837015     10.3822487651     16.0811568754
 0     7.7847929249      6.7158744189      3.3009898006
 F     5.7969945041     12.3426277000     14.6465267733
 F     5.6637060389      8.4207636549     14.6233709491
 F     3.8119959683     10.4032215442     13.5222561275
 F     7.6813287364     10.3797679233     13.5249406649
      &END COORD
      &KIND O
        ELEMENT O
        MASS    15.99940
      &END KIND
      &KIND Ti
        ELEMENT Ti
        MASS    47.867
      &END KIND
      &KIND F
        ELEMENT F
        MASS    18.998
      &END KIND
      &END SUBSYS
 STRESS_TENSOR ANALYTICAL
 &END FORCE_EVAL
```